Neurobiology of Disease 155 (2021) 105392

Contents lists available at ScienceDirect

Neurobiology of Disease

journal homepage: www.elsevier.com/locate/ynbdi

Inhibitory effects of xanthine oxidase inhibitor, topiroxostat, on development of neuropathy in db/db mice

Kazuhisa Takahashi [a,b], Hiroki Mizukami [a,*], Sho Osonoi [a,b], Saori Ogasawara [a], Yutaro Hara [a,c], Kazuhiro Kudoh [a], Yuki Takeuchi [a,b], Takanori Sasaki [a], Makoto Daimon [b], Soroku Yagihashi [a]

[a] Department of Pathology and Molecular Medicine, Hirosaki University Graduate School of Medicine, 5 Zaifu-cho, Hirosaki, Aomori 036-8562, Japan
[b] Department of Endocrinology and Metabolism, Hirosaki University Graduate School of Medicine, 5 Zaifu-cho, Hirosaki, Aomori 036-8562, Japan
[c] Department of Gastroenterological Surgery and Pediatric Surgery, Hirosaki University Graduate School of Medicine, 5 Zaifu-cho, Hirosaki, Aomori 036-8562, Japan

ARTICLE INFO

Keywords:
Diabetic neuropathy
Xanthine oxidase inhibitor
Macrophages
Oxidative stress
Inflammation
Type 2 diabetes

ABSTRACT

Inflammation and oxidative stress contribute to the pathophysiology of diabetic neuropathy. According to recent evidence, the modulation of macrophage polarization in peripheral nerves represents a potential therapeutic target for diabetic neuropathy. Xanthine oxidase, which is a form of xanthin oxidoreductase, is the rate-limiting enzyme that catalyzes the degradation of hypoxanthine and xanthine into uric acid. Activation of xanthine oxidase promotes oxidative stress and macrophage activation. A preclinical study reported the beneficial effects of xanthine oxidase inhibitors on peripheral nerve dysfunction in experimental models of diabetes. However, the detailed mechanisms remain unknown. In this study, we examined the effect of the xanthine oxidase inhibitor topiroxostat on macrophage polarization and peripheral neuropathy in an obese diabetic model, db/db mice. First, the effects of xanthine oxidase inhibitors on cultured macrophages and dorsal root ganglion neurons exposed to xanthine oxidase were assessed. Furthermore, five-week-old db/db mice were administered the xanthine oxidase inhibitors topiroxostat [1 mg/kg/day (dbT1) or 2 mg/kg/day (dbT2)] or febuxostat [1 mg/kg (dbF)]. Glucose metabolism and body weight were evaluated during the experimental period. At 4 and 8 weeks of treatment, peripheral nerve functions such as nerve conduction velocities, thermal thresholds and pathology of skin and sciatic nerves were evaluated. The mRNA expression of molecules related to inflammation and oxidative stress was also measured in sciatic nerves. Untreated db/db mice and the nondiabetic db strain (db/m) were studied for comparison. An in vitro study showed that topiroxostat suppressed macrophage activation and proinflammatory but not anti-inflammatory polarization, and prevented the reduction in neurite outgrowth from neurons exposed to xanthine oxidase. Neuropathic changes exemplified by delayed nerve conduction and reduced intraepidermal nerve fiber density developed in db/db mice. These deficits were significantly prevented in the treated group, most potently in dbT2. Protective effects were associated with the suppression of macrophage infiltration, cytokine expression, and oxidative stress in the sciatic nerve and decreased plasma xanthine oxidoreductase activity. Our results revealed the beneficial effects of the xanthine oxidase inhibitor topiroxostat on neuropathy development in a mouse model of type 2 diabetes. The suppression of proinflammatory macrophage activation and oxidative stress-induced damage were suggested to be involved in this process.

Abbreviations: DN, diabetic neuropathy; M1, proniflammatory macrophages; M2, anti-inflammatory macrophages; XOR, xanthine oxidoreductase; UA, uric acid; XO, xanthine oxidase; ROS, reactive oxygen species; T2D, type 2 diabetes mellitus; DMEM, Dulbecco's modified Eagle's medium; FBS, fetal bovine serum; IL-4, interleukin-4; LPS, lipopolysaccharide; DRG, dorsal root ganglia; OGTT, oral glucose tolerance test; ITT, insulin tolerance test; MNCV, motor nerve conductive velocity; SNCV, sensory nerve conductive velocity; TBARS, thiobarbituric acid-reactive substances; MDA, malondialdehyde; IL-1β, interleukin-1β; iNOS, inducible NO synthase; TNF-α, tumor necrosis factor-α; 8-OHdG, 8-hydroxy-2′-deoxyguanosine; IENFD, intraepidermal nerve fiber density; PGP9.5, protein gene product 9.5; NGF, nerve growth factor.

* Corresponding author.
E-mail address: hirokim@hirosaki-u.ac.jp (H. Mizukami).

https://doi.org/10.1016/j.nbd.2021.105392
Received 2 February 2021; Received in revised form 3 May 2021; Accepted 10 May 2021
Available online 14 May 2021

1. Introduction

Of all diabetic small vessel complications, diabetic neuropathy (DN) is the most prevalent and earliest to manifest (Feldman et al., 2017; Vinik et al., 2013; Yagihashi et al., 2011; Ziegler et al., 2014). Clinical data indicate that glycemic control is critical for reducing the risk of developing DN. Strict glycemic control reverses the reduction in small fibers, which is a characteristic of the initial stage of DN (Azmi et al., 2015; Mehra et al., 2007), while it has less efficacy on advanced-stage DN, in which large fibers are also abolished. Based on these findings, the mechanisms of DN might change during the progression from the initial stage to the chronic stage (Kudoh et al., 2020; Mizukami et al., 2020).

Macrophage infiltration and polarization are associated with the pathogenesis of diabetic complications, including DN (Conti et al., 2002; Fan et al., 2020; Juranek et al., 2013; Mizukami et al., 2011; Yamagishi et al., 2008). Activation of proinflammatory macrophages (M1) was recently observed in experimental animals with DN, while anti-inflammatory macrophage (M2) polarization was shown to ameliorate the symptoms of DN (Fan et al., 2020; Juranek et al., 2013). In the early stage of DN, macrophage migration to sciatic nerves is implicated in both the damage and regeneration of nerve tissues in an experimental model with DN (Conti et al., 2002). Conversely, in experimental models with chronic DN, macrophages infiltrate sciatic nerves and induce oxidative stress (Mizukami et al., 2011; Yamagishi et al., 2008). These results suggest that inflammation may shift during the progression of DN. However, the detailed mechanism is not fully understood.

Xanthine oxidoreductase (XOR) is the rate-limiting enzyme that catalyzes the degradation of hypoxanthine and xanthine into uric acid (urate, UA). Xanthine oxidase (XO), a form of XOR, is activated in chronic inflammation (Amaya et al., 1990; Ives et al., 2015) and promotes reactive oxygen species (ROS) generation (Okuda et al., 1996). XO inhibitors are clinically applied as treatments for hyperuricemia and gout. Blood XOR activity is increased in patients with diabetes (Furuhashi et al., 2018; Sunagawa et al., 2019). Inhibition of XO suppresses M1 macrophages accompanied by an improvement in insulin resistance (Nishikawa et al., 2020). The increase was also observed in patients with type 2 diabetes mellitus (T2D) presenting with DN but not in those without DN, indicating that it may serve as an independent predictor of DN (Miric et al., 2016). Treatment with high doses of allopurinol, an XO inhibitor, improves nerve conduction velocities, tactile allodynia, and thermal hyperalgesia in rats with experimental diabetes (Inkster et al., 2007). Thus, XO may be a potential therapeutic target for DN. However, the molecular mechanism underlying the role of XO in the pathophysiology of DN remains unknown.

In this study, we evaluated the effects of a new, selective XO inhibitor, topiroxostat, on DN in db/db mice, a suitable model for obese humans with T2D complicated with progressive neuropathy (Norido et al., 1984; O'Brien et al., 2015). We also explored the mechanism by which topiroxostat modulates the development of neuropathy in this model.

2. Materials and methods

2.1. Macrophage activation and effects of XO inhibitors

The macrophage cell line RAW264.7 was purchased from RIKEN Biosource Research Center (Ibaraki, Japan) and cultured in Dulbecco's modified Eagle's medium (DMEM) containing 5.6 mM glucose, 10% heat-inactivated fetal bovine serum (FBS), 100 U/mL penicillin, and 100 μg/mL streptomycin. After 24 h of starvation in 0.5% FBS-containing medium, RAW264.7 cells were first treated with 4.3 ng/mL XO inhibitors to diminish nonspecifically activated XO (Nakamura et al., 2019). One hour later, the XO pathway was activated by the addition of 0.005 U/mL XO (Merck KGaA, Darmstadt, Germany). For the morphological evaluation, macrophages were incubated with XO and/or XO inhibitors for 48 h and stained with an anti-panmacrophage antibody (CD68, Abcam plc., Cambridge, UK) and Alexa Fluor 565 secondary antibody (Thermo Fisher Scientific, MA, USA). Images were captured with an Axioimager A2 microscope (Carl Zeiss AG, Oberkochen, Germany). The circularity of the cell contour was evaluated with ImageJ v1.47 software (NIH, MD, USA). Forty cells from each group were repeatedly evaluated four times. For polarization to M1 macrophages, harvested cells were labeled with a FITC-conjugated B7–1/CD80 antibody (Proteintech Group, Inc., Rosemont, IL, USA). The incubated cells were analyzed using flow cytometry (FACSAria™ II instrument, BD Biosciences, NJ, USA). The results obtained with an American hamster IgG isotype control are shown in supplemental Fig. 1. The flow cytometry analysis was performed 3 times, and average values were compared. RAW264.7 cells were differentiated into the M2 phenotype with 0.125 μg/mL interleukin-4 (IL-4) (Merck KGaA) or the M1 phenotype with 1 mg/mL lipopolysaccharide (LPS) (Merck KGaA) in the presence or absence of simultaneous treatment with XO inhibitors for 30 h to evaluate the effects of XO inhibitors on polarized M1 or M2 macrophages. After culture, total RNA was purified from the cells, and mRNA expression was quantitatively evaluated, similar to the procedure used for sciatic nerves.

2.2. Cultured DRG neurons and the effect of XO inhibitors

Primary cultures of neurons isolated from the dorsal root ganglia (DRG) in the lumbar spinal cord of 5-week-old male db/m mice were prepared (Sango et al., 2008). Effects of XO inhibitors (4.3 ng/mL) on neurite outgrowth from DRG neurons exposed to 0.005 U/mL XO were evaluated using the method described in previous studies with modifications (Nakamura et al., 2019; Sango et al., 2008). After 1 h of preincubation with XO inhibitors, DRG neurons were cultured with or without XO for 48 h. The number of neurite-bearing cells was counted among all neurons in the well and expressed as a percentage (Sango et al., 2008). Neurite length was measured from digital images of the stained neurites using an image analysis system (ImageJ). The average length of the neurites (μm) was calculated from the measurements of approximately 60 neurites obtained from 4 to 5 different wells in each experimental group. For the critical evaluation of treatment effects, the number of neuronal cells at baseline was adjusted to approximately 600 in a delineated circle with a 1-cm diameter in each well at 16 h after seeding. Since cell density influences the neurite outgrowth and survival of neurons (Sango et al., 2011), these adjustments are required for the critical evaluation. Images of neuronal cells were acquired using a confocal laser scanning microscope (CQ1, Yokogawa Electric Corp., Tokyo, Japan).

2.3. Animal study

The Committee on Animal Care of Hirosaki University approved all the experiments conducted in this study (#M14006). The procedures followed the Principles of Laboratory Animal Care (National Institutes of Health publication no. 85–23, revised 1985) and the institutional guidelines of Hirosaki University Animal Experimentation for the care and use of laboratory animals.

Four-week-old male C57BLKS/J-$m^{+/+}Lepr^{db}$ homozygous (db/db) mice were used as a diabetic model, and heterozygous *db/lean* mice (db/m) obtained from CLEA Japan Inc. (Tokyo, Japan) were used as a control group and fed laboratory-standard powdered chow. Mice were allowed ad libitum access to food and water and housed in polycarbonate cages, each containing 4 mice, with wire lids and hardwood chips for bedding at a constant temperature (23 ± 2 °C) under a 12-h light–dark cycle (lights on: 7:00 a.m.–7:00 p.m.). At 5 weeks of age, diabetic mice were randomly categorized into four groups: an untreated control group (db), a group treated with low-dose topiroxostat (1 mg/kg/day) (dbT1), a group treated with high-dose topiroxostat (2 mg/kg/day) (dbT2), and a group treated with febuxostat (1 mg/kg/day) (dbF). Each group was

housed in the same cage and received either drug- or vehicle-containing food for 4 or 8 weeks. The doses of topiroxostat and febuxostat were determined based on previous reports while incorporating safety margins (Honorat et al., 2013; Nakamura et al., 2016). During the experimental period, food intake was measured at an interval of one to four days, and body weight was evaluated once a week. The dose of compound in the mixture of ground food was calculated using the following formula:

$$\begin{aligned} &\textit{Dose of compounds } (mg/100\,g\,food) = 1 \textit{ or } 2\ mg \\ &\textit{of compound x average body weight of each mouse} \\ &\textit{per cage } (g)\ \ x\,0.001/\textit{food intake}\ \ (g/day/mouse)\ x\ 100 \end{aligned}$$

The adjusted food mixture was set and measured at 9:00 AM. All mixtures of food and compound were recovered, even if the mixture was spread out from the feeder as much as possible. If the mixture was wet with urine, the weight was evaluated after it was dry. We confirmed the lack of toxic effects on body weight, food intake and glucose metabolism and the absence of xanthine deposition in the kidney in db/m mice (Suppl. Fig. 1). Potent inhibitory activity of topiroxostat and febuxostat at a dose of 2–5 mg/kg/day was reported in a previous study (Nakamura et al., 2016). Blood glucose levels were measured weekly. Mice were fed reconstructed chow mixtures such that they received the ideal dose of either topiroxostat or febuxostat throughout the experimental period. A 2 g/kg oral glucose tolerance test (OGTT) and 1 U/kg insulin tolerance test (ITT) were conducted at 0, 4, and 8 weeks of the experimental period. During the challenge test, blood was obtained from the tail. Insulin concentrations were measured in plasma samples stored in heparinized tubes at −75 °C using enzyme-linked immunosorbent assay (ELISA) kits (Morinaga Biol. Sci., Yokohama, Japan). Finally, the mice were euthanized with 3% isoflurane anesthesia after an overnight fast (16 h) in the animal facility of Hirosaki University School of Medicine. One hundred-seventeen mice were euthanized, including 8 mice (4 mice per group) at the starting point, 55 mice (11 mice per group) at 4 weeks of treatment and 54 mice (7–9 mice per group) at 8 weeks of treatment. Blood samples were centrifuged at 2000 xg for 20 min to obtain blood plasma. Sciatic nerve, DRG, and hind limb footpad skin were also dissected. Plasma, partial segments of the sciatic nerve, and DRG tissues were stored at −80 °C.

2.4. Assessment of peripheral nerve function

At 4 and 8 weeks after treatment, the motor nerve conduction velocity (MNCV) and sural sensory nerve conduction velocity (SNCV) were measured (Guo et al., 2020; Tsuboi et al., 2016). During the assessment, mice were placed on a thermostatically controlled heated mat to maintain the body temperature at 37 °C. The temperature near the sciatic nerve was also maintained at constant value of 37 °C with the aid of a warmed blanket and monitoring with an electronic thermometer (PC-9400 Delta; Sato Keiryoki MFG, Tokyo, Japan). An average value of 5 recordings was considered representative of each animal.

The tail flick response to the thermal stimulus of radiant heat was measured using the TAIL FLICK ANALGESIA METER (Morimachi Kikai Co., Ltd., Tokyo, Japan) (Guo et al., 2020). Briefly, the animal was gently wrapped in a towel and placed on the top of the instrument with the tail in the sensing groove. The tail flick latency was determined by exposing the animal's tail to a radiant heat source and recording the time taken to remove the tail from the noxious thermal stimulus. The radiation intensity was chosen based on the intensity required to elicit a basal tail flick response of 2 to 3 s in control mouse of 13 weeks of ages. The temperature for stimulation was set to 56 °C. The tail flick latencies were measured 10 times per session at a minimum interval of 10 min. Tail movements due to voluntary locomotion were excluded from the measurement.

2.5. Measurement of oxidative stress products

The thiobarbituric acid-reactive substance (TBARS) measurement was based on malondialdehyde (MDA) accumulation evaluated using the TBARS assay kit (Cayman Chemical, MI, USA) according to the manufacturer's instructions; 0.005 U/mL XO (Merck KGaA) was incubated with 100 μmol/L xanthine or hypoxanthine in DMEM for 1 h at 37 °C. Hydroperoxide production in the medium and serum was evaluated with Amplex Red according to the manufacturer's instructions (Thermo Fisher Scientific).

2.6. Measurement of UA concentrations

Concentrations of UA in plasma, sciatic nerve, and DRG were measured (Nakamura et al., 2016). Briefly, tissues were homogenized in phosphate-buffered saline (PBS) (pH 7.4) and centrifuged at 20,000 xg at 4 °C for 20 min. These homogenates or blood plasma were added to a methanol solution containing [$^{13}C_2$, $^{15}N_2$] UA as an internal standard and centrifuged at 3000 xg at 4 °C for 20 min. Following dilution with distilled water, the supernatant was subjected to analysis with liquid chromatography-triple quadrupole mass spectrometry (LC-TQMS, Nexera, Shimadzu-QTRAP4500, SCIEX, Tokyo, Japan).

2.7. XOR activity in plasma, sciatic nerve, and DRG

XOR activities in the sciatic nerve, DRG and blood plasma were measured using a previously described method (Murase et al., 2016) with some modifications. Briefly, following homogenization and centrifugation (20,000 xg, 4 °C, 10 min), the tissues were incubated with a mixture containing [$^{13}C_2$, $^{15}N_2$] xanthine as the substrate, NAD^+, and oxonate in 20 mmol/L Tris buffer (pH 8.5) at 37 °C for 30 min. Thereafter, methanol containing [$^{13}C_3$, $^{15}N_3$] UA was added as an internal standard. The mixtures were subsequently centrifuged at 3000 xg at 4 °C for 20 min. The supernatants were evaporated, reconstituted with distilled water, and filtered through ultrafiltration membranes (AcroPrep™ Advance 96-Well Filter Plates for Ultrafiltration, Omega™ 3 K MWCO, Pall Corp. NY, USA). The concentration of [$^{13}C_2$, $^{15}N_2$] UA was measured using LC-TQMS (Nexera-QTRAP4500). XOR activity was reported as [$^{13}C_2$, $^{15}N_2$] UA production in pmol/min/mg of total protein.

2.8. Quantitative evaluation of the mRNA expression of inflammatory cytokines

Total RNA was extracted from the stored frozen tissues or cell lysates with Isogen II (Nippon Gene Co., Ltd., Tokyo, Japan). Subsequently, cDNAs were generated with the SuperScript® VILO cDNA Synthesis Kit (Thermo Fisher Scientific) and used as a template for real-time PCR (Takahashi et al., 2012). Commercially available primer and probe sets (gene expression assays, Thermo Fisher Scientific) for target genes of interleukin-1β (IL-1β), inducible nitric oxide synthase (iNOS), tumor necrosis factor-α (TNF-α), arginase I, and the internal standard β2 microglobulin were mixed with cDNAs and Thunderbird Probe qPCR Mix (Toyobo Co. Ltd., Osaka, Japan). An established RT-PCR assay using the relative quantification method (ΔΔCT) was conducted in an ABI PRISM 7000 Sequence Detection System (Thermo Fisher Scientific). The threshold cycle of each gene was determined as the number of PCR cycles at which an increase in reporter fluorescence was detected above a baseline signal. The difference in threshold cycles between the target gene and β2 microglobulin yields the standardized expression level (ΔCt). Subtraction of ΔCt of the control from ΔCt of the targeted groups generates the ΔΔCt value that was used to calculate relative expression levels in targeted groups with the formula $2^{-\Delta\Delta Ct}$. The expression levels of each gene are reported as the fold increase in targeted groups compared with the control.

2.9. Pathological evaluation

Sciatic nerves and DRG were fixed with 10% buffered formalin and embedded in paraffin; 4 μm-thick sections were subjected to immunofluorescence and immunoperoxidase staining (Guo et al., 2020; Mizukami et al., 2020). Supplemental Table 1 shows a list of applied primary and secondary antibodies. Because the species of the antibodies against XOR (Abcam plc.) and Factor VIII (Agilent, CA, USA) was identical, mirror-image sections were separately stained for each antibody with different colors, and merged images were obtained using a confocal laser scan microscope (CQ1). The specificity was confirmed by replacing the primary antibodies with nonimmune sera or omitting the primary antibodies. The number of cells stained with an antibody against iNOS for proinflammatory macrophages (M1) (Abcam plc.), CD206 for anti-inflammatory macrophages (M2) (Abcam plc.), and 8-hydroxy-2′-deoxyguanosine (8-OHdG) (Nihon Yushi corp., Kumamoto, Japan) for ROS-induced DNA damage was counted in the whole area of one cross-sectional surface of the sciatic nerve. Two sections with 20 μm intervals per sample were evaluated for each animal. The numbers of iNOS-positive M1 and CD206-positive M2 macrophages are reported as the average numbers of positive cells per unit area. Fluorescent positive reaction with DAPI positive nucleus was regarded as labeled macrophages. For the evaluation of 8-OHdG-positive cells, immunostained transverse-sections of the sciatic nerve were subjected to an ImageJ analysis (Mizukami et al., 2011; Yamagishi et al., 2008). Cells positive for 8-OHdG were identified as strongly positive, and their intensity was more than two times that of the background intensity evaluated using ImageJ software. The average percentage of positive cells was reported as an index of positivity (%). We obtained 15.4 ± 2.4 images at x 40 magnification for each nerve. The average number of cells counted in each obtained image was 114.6 ± 29.3 for 8-OHdG staining, 4.9 ± 3.3 for CD206 staining, and 20.2 ± 19.0 for iNOS staining.

For an objective comparison of the staining results among groups, sciatic nerve sections from each group were mounted on a single slide (i.e., 5 sciatic nerve tissues on one slide), stained under the same conditions, and counted separately by three researchers who were blinded to the groups (KT, SO, and KK).

2.10. Evaluation of intraepidermal nerve fiber density

The intraepidermal nerve fiber density (IENFD) was evaluated using immunofluorescence staining (Guo et al., 2020; Mizukami et al., 2020). The skin of hind foot pads from the plantar surface of the hind paw of both the left and right sides was fixed at 4 °C with Zamboni's fixative (2% paraformaldehyde and 0.2% picric acid in 0.1 M phosphate buffer) for 6–8 h, rinsed with 30% sucrose in PBS overnight, cryoembedded in mounting media, and sectioned at a 30 μm thickness. Epidermal nerve fibers were labeled with an anti-protein gene product 9.5 (PGP9.5) antibody (Agilent), and dermis was labeled with an anti-CK 5/6 antibody (Agilent) and incubated with secondary antiserum conjugated with different fluorophores (AlexaFluor 488 and 594, Thermo Fisher Scientific). Approximately 16 sequential images were captured at intervals of 2 μm and flattened in each frame with Axioimager A2 (Carl Zeiss). An average of 5 frames were evaluated per section, and three sections were measured for each footpad. IENFD data are presented as the mean number of fibers per linear mm of epidermis from a total of six sections per animal.

2.11. Statistical analyses

Data are presented as the means±standard deviations (SD). Statistical comparisons of the mean values among the groups were performed using analysis of variance with Tukey's test, and Student's or Welch's *t*-test was performed for parametric or nonparametric comparisons between the two groups (db/m and db, or db with or without treatment, respectively), using Jmp10.0.2 (SAS Institute Inc., Cary, NC, USA); a p value of 0.05 was considered statistically significant.

3. Results

3.1. Effects of the XO inhibitor on macrophages in vitro (Fig. 1)

Topiroxostat alone had no effect on the appearance of RAW264.7 cells (Fig. 1A). In contrast, the cells displayed ameboid, dendritic or ramified contours and formed multinucleated giant cells upon exposure to 0.005 U/mL XO with 100 μmol/L xanthine. This effect was reversed by the addition of 4.3 ng/mL topiroxostat to the medium (Fig. 1A). The circularity of the cell contour was reduced by XO stimulation ($p < 0.01$) (Fig. 1B). XO inhibitors prevented the reduction in circularity elicited by XO exposure ($p < 0.01$). Treatment with the XO inhibitor alone had no effect on the increase in the mRNA expression of the M1 markers TNF-α, IL-1β and iNOS in RAW264.7 cells (Fig. 1C). Exposure to XO with 100 μmol/L xanthine significantly increased the mRNA expression of M1 markers compared with the values of nonstimulated cells ($p < 0.01$). Coadministration of XO with topiroxostat or febuxostat significantly reduced the levels of the transcripts listed above (for all, $p < 0.01$). The flow cytometry analysis confirmed that XO inhibitors did not increase the polarization of macrophages into M1 macrophages (Fig. 1D–E). XO significantly increased the frequency of cells polarized to CD80-positive M1 ($p < 0.01$ compared with C). Both XO inhibitors significantly suppressed macrophage polarization induced by XO ($p < 0.01$ compared with C). LPS (1 mg/mL) also significantly increased the expression of M1 markers ($p < 0.01$) (Suppl. Fig. 3A). Both XO inhibitors significantly reduced the expression of these markers ($p < 0.01$ compared with LPS + T and $p < 0.05$ compared with LPS + F). IL-4 stimulation (0.125 μg/mL) significantly increased the mRNA expression of arginase I, an M2 marker, in RAW264.7 cells ($p < 0.01$) (Suppl. Fig. 3B). In contrast to M1 polarization, neither XO inhibitor affected M2 polarization. Measurement of the oxidized product revealed an increased concentration of hydrogen peroxide after a 2 h incubation with xanthine or hypoxanthine ($p < 0.01$) (Fig. 1F). Coadministration of XO with topiroxostat significantly inhibited the production of hydrogen peroxide ($p < 0.01$).

3.2. Effects of the XO inhibitor on DRG neurons (Fig. 2)

The neuronal cell survival rate after isolation was comparable among all groups (Fig. 2A). XO inhibitors did not exert direct effects on the population of neurite-bearing cells or neurite length. The addition of XO to cultured DRG neurons did not alter the rate of neuronal cell survival but significantly reduced the population of neurite-bearing cells and the average neurite length ($p < 0.01$) (Fig. 2B-C). Coadministration of topiroxostat with XO did not alter neuronal cell survival but significantly, although partially, protected the population of neurite-bearing cells and reduced neurite length ($p < 0.05$).

3.3. Laboratory findings and food intake of mice (Table 1)

The body weight of dbT2 mice at 8 weeks was significantly lower than that of db mice (38.3 ± 3.9 g vs. 44.1 ± 4.1 g, $p < 0.05$). Febuxostat treatment (dbF) did not alter the body weight or food intake. Food intake by dbT2 mice was decreased by 11% compared with db mice ($p < 0.05$). Blood glucose levels measured in either the fasting or nonfasting state were significantly higher in db mice than in db/m mice ($p < 0.01$). A significant increase in fasting blood glucose levels was observed in mice treated with topiroxostat (dbT1 and dbT2) and febuxostat (dbF) at 8 weeks compared with db mice ($p < 0.01$). In contrast, no significant difference in nonfasting blood glucose levels was observed in db mice treated with or without XO inhibitors. HbA1c levels in db mice were significantly increased compared with those in db/m mice ($p < 0.01$). Treatment with XO inhibitors did not affect the elevated HbA1c levels in db mice. Fasting plasma insulin levels were significantly increased in db mice compared to db/m mice ($p < 0.01$). XO inhibitors had no effect on

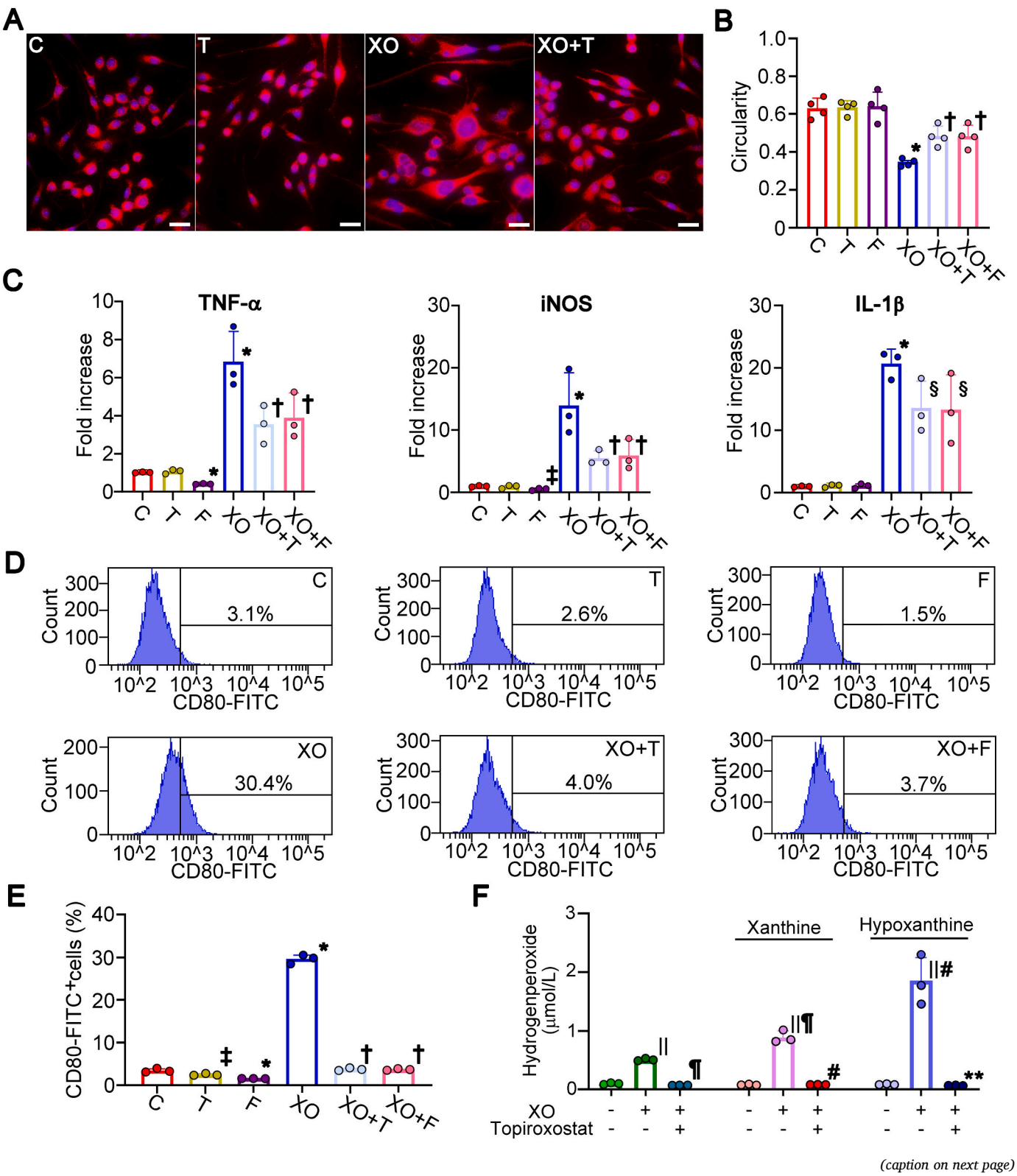

(caption on next page)

Fig. 1. Activation of macrophages exposed to XO.
RAW264.7 cells were cultured with topiroxostat and XO (**A**). The morphology of the cells remained unaffected after treatment with topiroxostat alone. In contrast, exposure to 0.005 U/mL XO altered the cellular shape into ameboid, dendritic, or ramified contours and induced the formation of multinucleated giant cells. The addition of 4.3 ng/mL topiroxostat partially suppressed the morphological changes in RAW264.7 cells induced by XO. The circularity of the RAW264.7 cell contour was unaffected by XO inhibitors (**B**). XO significantly reduced circularity ($p < 0.01$), while XO inhibitors prevented the reduction in circularity elicited by XO ($p < 0.01$ compared with XO). Under basal conditions prior to XO exposure, topiroxostat had no effect on gene expression, whereas febuxostat suppressed the expression of TNF-α and iNOS ($p < 0.01$ and $p < 0.05$, **C**). Exposure to XO significantly increased the expression of TNF-α, iNOS, and IL-1β ($p < 0.01$). Coadministration of topiroxostat or febuxostat with XO significantly suppressed the increased expression of these proinflammatory genes ($p < 0.01$) (**C**). The FACS analysis revealed that XO inhibitors decreased the frequency of CD80-positive cells ($p < 0.05$C vs. T and $p < 0.01$C vs. F). (**D–E**) XO significantly increased the frequency of CD80-positive cells ($p < 0.01$ compared with C), while XO inhibitors suppressed the increase ($p < 0.01$ for both). XO exposure also increased hydrogen peroxide generation in the culture medium ($p < 0.01$) (**F**), and this increase was suppressed by topiroxostat ($p < 0.01$). In the presence of 100 μmol/L xanthine or hypoxanthine, XO stimulation further increased hydrogen peroxide generation ($p < 0.01$). This effect was completely suppressed by topiroxostat ($p < 0.01$). Values are presented as means±SD. C, non-stimulated cells; T, topiroxostat; F, febuxostat; XO, xanthine oxidase; FACS, fluorescence-activated cell sorting. *$p < 0.01$ compared with C, $^{\dagger}p < 0.01$ compared with XO, $^{\ddagger}p < 0.05$ compared with C, $^{\S}p < 0.05$ compared with XO, $^{||}p < 0.01$ compared with XO(−)topiroxostat(−), $^{\P}p < 0.01$ compared with XO(+)topiroxostat(−), $^{\#}p < 0.01$ compared with XO + xanthine, and **$p < 0.01$ compared with XO + hypoxanthine. The scale bar represents 20 μm.

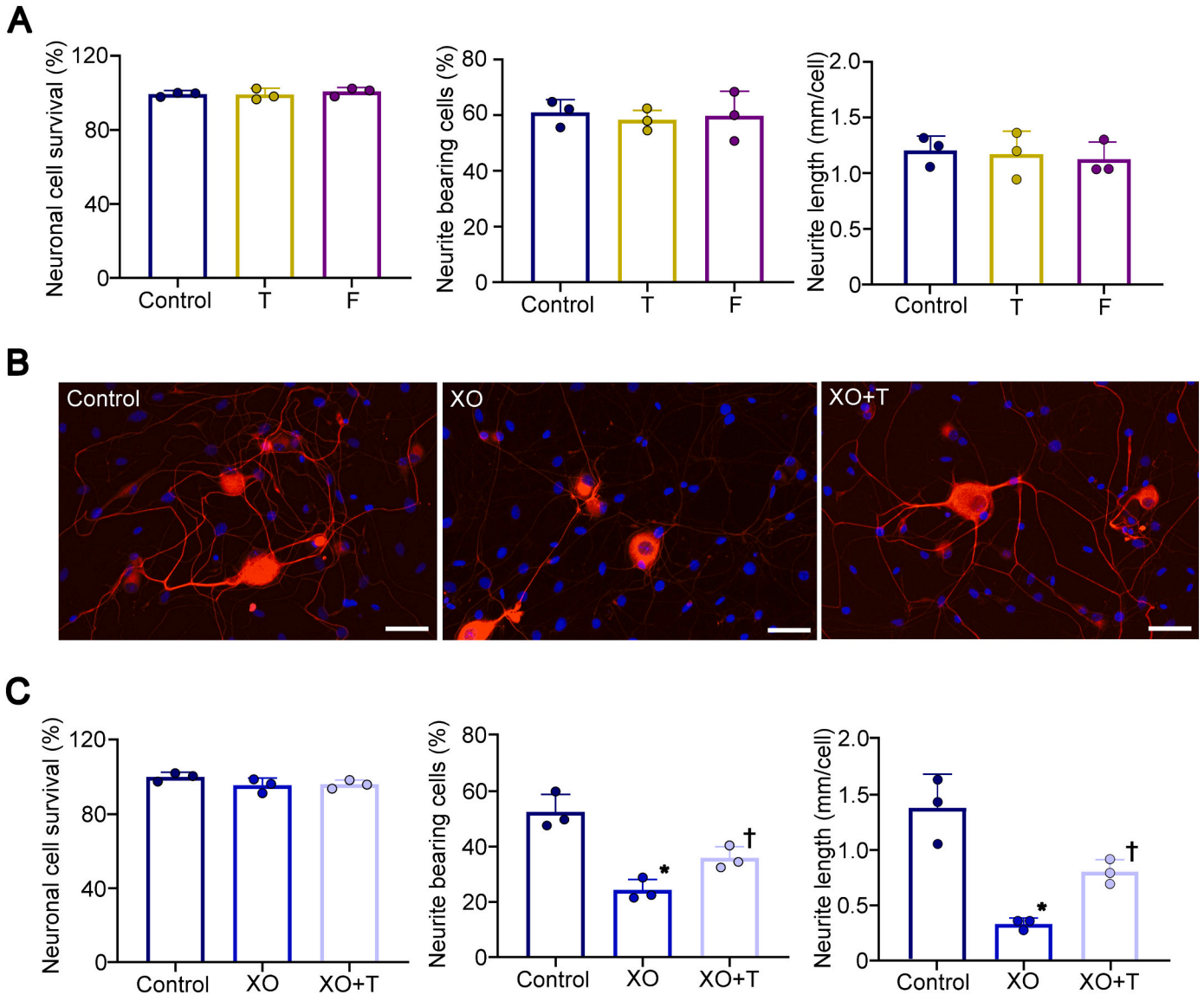

Fig. 2. Neurite outgrowth of DRG neurons and effects of XO.
DRG neurons isolated from db/m mice were cultured to evaluate neurite outgrowth. Neuronal cell survival, the frequency of neurite-bearing cells and neurite length were not affected by the addition of 4.3 ng/mL topiroxostat (T) and 4.3 ng/mL febuxostat (F) **(A)**, as depicted by β-tubulin III immunostaining (**B**, red: β-tubulin III, blue DAPI). In contrast, exposure to 0.005 U of XO significantly decreased the frequency of neurite-bearing cells and neurite length ($p < 0.01$ compared with the Control) (**B–C**). Topiroxostat significantly suppressed this reduction ($p < 0.05$ compared with XO). Values are presented as means±SD. T, topiroxostat; F, febuxostat; XO, xanthine oxidase. *$p < 0.01$ compared with the Control and $^{\dagger}p < 0.05$ compared with XO. The scale bar represents 50 μm. (For interpretation of the references to colour in this figure legend, the reader is referred to the web version of this article.)

Table 1
Clinical parameters of experiment animals.

	db/m	db	dbT1	dbT2	dbF
Body weight (g)					
Start (0 weeks)	21.4 ± 0.9 (*n* = 8)	28.8 ± 0.5* (*n* = 8)	29.1 ± 1.5* (*n* = 7)	28.6 ± 1.2* (n = 8)	28.9 ± 0.5* (n = 7)
End (8 weeks)	27.8 ± 1.5 (n = 7)	44.1 ± 4.1* (n = 8)	42.1 ± 3.6 (n = 7)	38.3 ± 3.9† (n = 8)	43.1 ± 4.2 (n = 7)
Food intake (g/day)					
Start (0 weeks)	3.3 ± 0.3 (n = 8)	5.7 ± 0.2* (n = 8)	5.6 ± 0.2* (n = 7)	5.6 ± 0.2* (n = 8)	5.7 ± 0.2* (n = 7)
End (8 weeks)	3.5 ± 0.4 (n = 7)	6.3 ± 0.5* (n = 8)	6.0 ± 0.2 (n = 7)	5.6 ± 0.5†‡ (n = 8)	6.4 ± 0.7 (n = 7)
Fasting blood glucose (mmol/L)					
Start (0 weeks)	4.6 ± 0.3 (n = 4)	10.8 ± 4.6§ (*n* = 4)	11.0 ± 3.9§ (n = 7)	10.2 ± 4.2§ (n = 8)	10.1 ± 3.8§ (n = 7)
End (8 weeks)	3.2 ± 0.3 (n = 7)	9.9 ± 2.3* (n = 8)	13.3 ± 1.9‖ (n = 7)	13.5 ± 3.2‖ (n = 8)	15.3 ± 2.3‖ (n = 7)
Nonfasting blood glucose (mmol/L)					
Start (0 weeks)	13.4 ± 1.5 (n = 4)	23.5 ± 7.6§ (n = 4)	21.8 ± 7.0§ (n = 7)	24.1 ± 5.8§ (n = 8)	23.0 ± 7.2§ (n = 7)
End (8 weeks)	8.1 ± 0.3(n = 7)	31.8 ± 2.3* (n = 8)	33.3 ± 0* (n = 7)	33.0 ± 1.0* (n = 8)	32.9 ± 1.0* (n = 7)
HbA1c (%) (8 weeks)	3.0 ± 0.0 (n = 7)	6.9 ± 0.7* (n = 8)	6.8 ± 0.6* (n = 7)	6.7 ± 1.1* (n = 8)	6.7 ± 0.8* (n = 7)
Fasting plasma insulin (ng/mL)					
End (8 weeks)	0.4 ± 0.3 (n = 7)	1.8 ± 0.3* (n = 8)	1.7 ± 0.1* (n = 7)	1.8 ± 0.2* (n = 8)	1.9 ± 0.1* (n = 7)

db/m, untreated db/m mice; db, db/db mice; dbT1, 1 mg/kg topiroxostat-treated db mice; dbT2, 2 mg/kg topiroxostat-treated db mice; dbF, febuxostat-treated db mice. Values are presented as means±SD. *p < 0.01 compared with db/m mice, †p < 0.05 compared with db mice, ‡p < 0.05 compared with dbT1 mice, §p < 0.05 compared with db/m mice, ‖p < 0.01 compared with db mice.

fasting plasma insulin levels.

3.4. OGTT and ITT (Suppl. Fig. 4)

At the beginning of the experiment, db mice showed a slight but significant aggravation of glucose tolerance in the OGTT and ITT compared to db/m mice (Suppl. Fig. 4A). Since the fed glucose level of db mice was greater than 22 mM despite the mild aggravation of the OGTT and ITT, db mice were regarded as having diabetes at the beginning of the experiment. At 4 and 8 weeks, db mice showed marked postchallenge hyperglycemia that was sustained from 30 min to 120 min **(**Suppl. Fig. 4B–C**)**. XO inhibitors did not exert a significant effect on glucose tolerance in db mice. The ITT revealed a gradual attenuation of insulin tolerance in db mice with aging compared to db/m mice ($p < 0.01$) **(**Suppl. Fig. 4B–C**)**. Insulin resistance was not significantly affected by XO inhibitors in db mice.

3.5. Assessment of peripheral nerve function (Table 2)

SNCV and MNCV were comparable between db/m and db mice at the start of the experiment. Significant delays in both SNCV and MNCV were observed in db mice compared to db/m mice at 4 and 8 weeks ($p < 0.01$, respectively); the delay was significantly prevented in dbT2 mice at both 4 and 8 weeks ($p < 0.05$). The effects of treatment with either a low dose of topiroxostat (dbT1) or febuxostat (dbF) were equivocal.

The tail flick test did not reveal an obvious change in the pain threshold of db mice in response to thermal stimuli at 0 week and 4 weeks of treatment; however, the pain threshold was significantly elevated at 8 weeks ($p < 0.01$). Mice in the dbT2 group showed an improvement in this response ($p < 0.01$), and the responses were modestly improved in the other treatment groups (p < 0.05 compared with db, respectively).

3.6. In situ macrophage infiltration in the sciatic nerve (Fig. 3)

Only a few macrophages were detected on the cross-sections of the sciatic nerve in both db and db/m mice at baseline, and differences in M1 (iNOS positive) and M2 (CD206 positive) ratios between these two groups were not significant (Fig. 3A–D). At 4 weeks of treatment, however, the number of M1 cells was markedly increased in db mice compared to db/m mice ($p < 0.01$) (Fig. 3A and C). This increase was suppressed by topiroxostat treatment in a dose-dependent manner. Febuxostat treatment similarly suppressed M1 macrophage infiltration. Compared to 4 weeks, the extent of M1 macrophage infiltration decreased at 8 weeks but remained greater in db mice than in db/m mice (p < 0.01) (Fig. 3B–C). The suppression of M1 macrophage infiltration at 8 weeks, although still greater than the infiltration observed in db/m mice, was also detected in the dbT2 and dbF groups ($p < 0.01$ and 0.05, respectively). M2 macrophage infiltration was comparable among all the groups at 4 weeks (Fig. 3A and D). In contrast, M2 macrophage infiltration was significantly decreased in db mice at 8 weeks compared to db/m mice, and this decrease was not altered in any of the treated groups (Fig. 3B and D). The ratio of M1/M2 macrophages gradually increased in db mice, and this increase was suppressed in the dbT2 and dbF groups **(**Fig. 3E**)**.

3.7. RT-PCR of inflammatory molecules in the sciatic nerve (Fig. 4)

Only a trend toward an increase in the expression of the TNF-α and

Table 2
Nerve function of experimental animals.

	MNCV (m/s)			SNCV (m/s)			Thermal threshold (s)		
Duration (weeks)	0	4	8	0	4	8	0	4	8
db/m	32.6 ± 2.5	34.8 ± 2.8	39.8 ± 1.8	30.2 ± 1.1	32.2 ± 2.1	35.1 ± 2.1	4.8 ± 0.7	4.8 ± 0.8	2.5 ± 0.5
db	31.1 ± 2.9	29.6 ± 3.4*	30.0 ± 2.2*	29.7 ± 1.8	28.7 ± 1.5*	30.9 ± 1.2*	4.9 ± 0.6	4.9 ± 0.9	4.5 ± 0.8*
dbT1	33.4 ± 2.7	29.5 ± 2.0*	30.7 ± 3.2*	31.0 ± 1.5	27.9 ± 1.0*	30.3 ± 1.5*	3.9 ± 0.8	4.7 ± 0.6	3.9 ± 0.5†
dbT2	30.3 ± 3.1	32.2 ± 1.5†‡	33.0 ± 4.6†	30.3 ± 1.6	30.6 ± 1.5†§	32.8 ± 1.4†§	4.8 ± 0.7	4.8 ± 1.0	2.9 ± 0.5‡‖
dbF	32.0 ± 3.0	29.5 ± 2.1¶	31.6 ± 1.8*	29.5 ± 1.5	27.4 ± 1.4¶	31.0 ± 1.3*	5.3 ± 0.9	4.9 ± 0.8	3.9 ± 0.5†#

MNCV, motor nerve conduction velocity; SNCV, sensory nerve conduction velocity; db/m, untreated db/m mice; db, db/db mice; dbT1, 1 mg/kg topiroxostat-treated db mice; dbT2, 2 mg/kg topiroxostat-treated db mice; dbF, febuxostat- treated db mice. Values are presented as means±SD.*p < 0.01 compared with db/m mice, †p < 0.05 compared with db mice, ‡p < 0.05 compared with dbT1 mice, §p < 0.01 compared with dbT1 mice, ‖p < 0.01 compared with db mice, ¶p < 0.01 compared with dbT2 mice, #p < 0.05 compared with dbT2 mice.

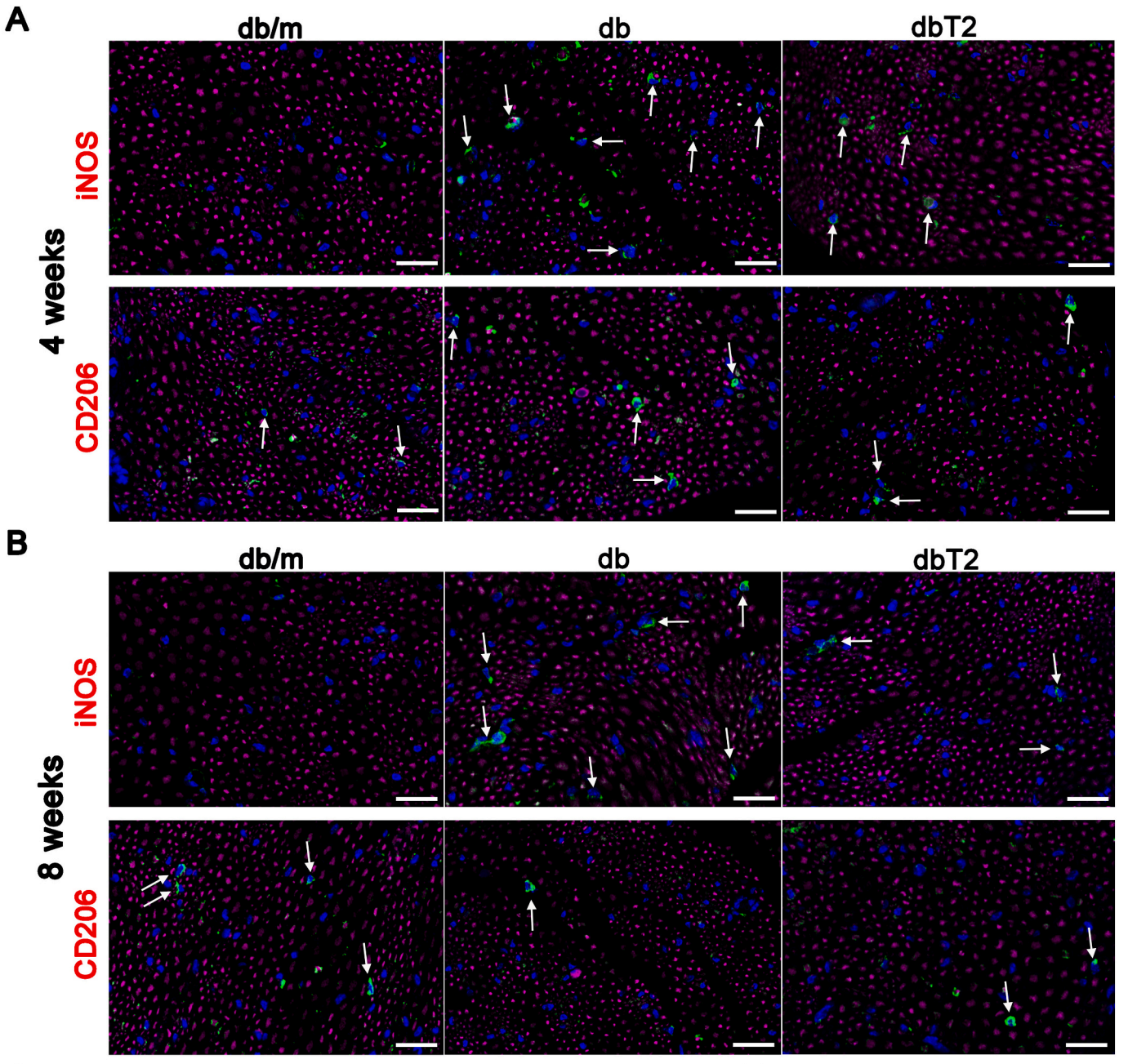

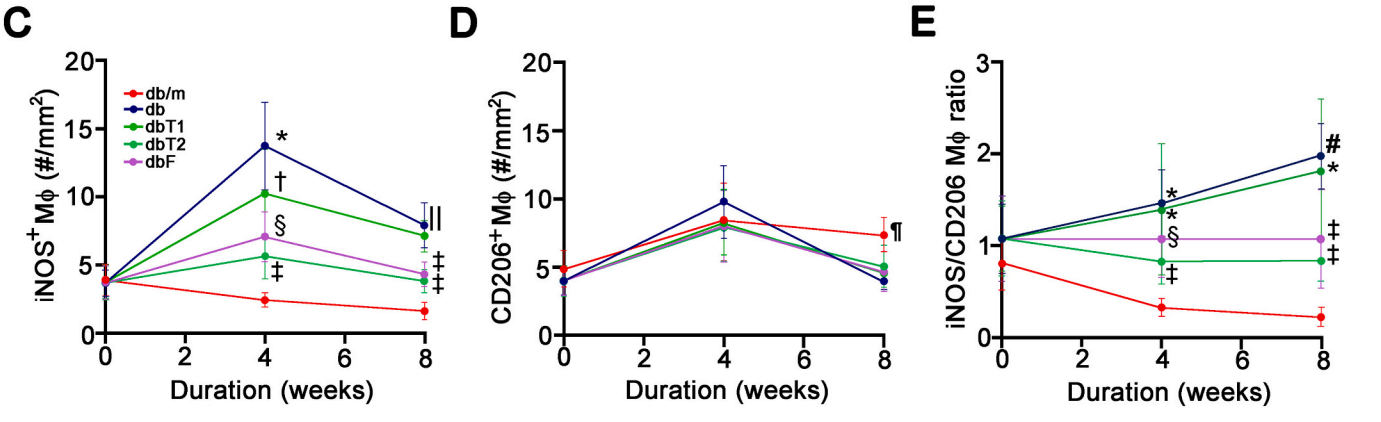

(caption on next page)

Fig. 3. Macrophage infiltration in the sciatic nerve.
Proinflammatory M1 macrophages labeled with an anti-iNOS antibody and anti-inflammatory M2 macrophages labeled with an anti-CD206 antibody were visualized as showing green fluorescence (**A–B**). Nerve fibers were labeled with an antibody against β-tubulin III (purple). A significant increase in the number of M1 macrophages was observed in db mice at 4 weeks compared to db/m mice. This increase was significantly suppressed in the groups treated with high doses of topiroxostat (dbT2) and febuxostat (dbF) ($p < 0.01$ dbT1 vs. dbT2, $p < 0.05$ dbT1 vs. dbF). M1 macrophage infiltration at 8 weeks was substantially reduced compared to that at 4 weeks but was still sustained in db mice at a significantly higher level than in db/m mice (**B–C**). The dbT2 and dbF groups continued to show reduced M1 infiltration at 8 weeks ($p < 0.01$ compared with the dbT1 group). In contrast, the extent of M2 macrophage infiltration was comparable among all the groups at 4 weeks (**A and D**). At 8 weeks, the number of M2 macrophages in db mice was significantly decreased compared with those in db/m mice, and this difference was not affected by XO inhibitors (**B and D**). Serial changes in the ratio of M1 to M2 macrophages are illustrated **(E).** Values are presented as means±SD. db/m, untreated db/m mice; db, db/db mice; dbT1, 1 mg/kg topiroxostat-treated db mice; dbT2, 2 mg/kg topiroxostat-treated db mice; dbF, febuxostat-treated db mice. $^{*}p < 0.01$ compared with db/m mice, $^{\dagger}p < 0.05$ compared with db mice, $^{\ddagger}p < 0.01$ compared with the dbT1 group, $^{\S}p < 0.05$ compared with the dbT1 group, $^{||}p < 0.01$ compared with db/m and db mice (4 weeks), $^{\P}p < 0.01$ compared with the db, dbT1, dbT2 and dbF groups, $^{\#}p < 0.01$ compared with db/m mice, and $p < 0.05$ compared with db mice (4 weeks). The scale bar represents 20 μm. (For interpretation of the references to colour in this figure legend, the reader is referred to the web version of this article.)

iNOS mRNAs was observed in db mice compared to db/m mice at the start of the experiment(Fig. 4A). At 4 weeks, the expression of the TNF-α, IL-1β, and iNOS mRNAs was 4–12 times higher in db mice than in db/m mice ($p < 0.01$) (Fig. 4B). The increase in the expression of the aforementioned proinflammatory genes was only partially suppressed in the dbT1 group but significantly suppressed in the dbT2 group ($p < 0.01$ for TNF-α and iNOS, and $p < 0.05$ for IL-1β). The effects of the XO inhibitor treatment were sustained but less pronounced at 8 weeks **(**Fig. 4C**).** Arginase I mRNA expression, a marker of the M2 phenotype, was comparable between db and db/m mice at baseline and at 4 weeks among all groups (Fig. 4A–B). At 8 weeks, however, its expression was significantly decreased compared to db/m mice ($p < 0.01$) (Fig. 4C). The XO inhibitor treatment did not significantly alter arginase I mRNA expression.

3.8. IENFD (Fig. 5)

IENFD was comparable between db/m and db mice treated with or without the XO inhibitor at 4 weeks of treatment (Fig. 5A and C). At 8 weeks, IENFD was significantly decreased in db mice compared with db/m mice ($p < 0.01$) (Fig. 5B and D), and the IENFD in the dbT2 group was comparable to db/m mice, showing significant protection of nerve fiber loss in the dbT2 group. The value in the dbF group was similar to that in untreated db mice.

3.9. ROS production in the sciatic nerve (Fig. 6)

At 4 weeks of treatment, 8-OHdG-positive reactions were identified frequently in endothelial cells, Schwann cells, and macrophages in the sciatic nerve of db mice (Fig. 6A). The number of 8-OHdG-positive cells was decreased in the dbT2 and dbF groups compared to db mice at 4 weeks ($p < 0.01$) (Fig. 6A-B). A similar trend was observed at 8 weeks ($p < 0.01$ db mice vs. dbT2 mice and $p < 0.05$ db mice vs. dbF mice) (Fig. 6B). The tissue concentration of MDA was significantly increased in db mice compared to db/m mice at both 4 weeks and 8 weeks ($p < 0.01$) (Fig. 6C). This increase was inhibited in the dbT1 and dbT2 groups in a dose-dependent manner. The suppressive effect on MDA levels was less marked in the dbF group. At 8 weeks, only the dbT2 group showed a significant reduction in MDA levels among all the groups ($p < 0.05$ compared with db mice). Blood hydrogen peroxide levels were significantly elevated in db mice compared to db/m mice at 8 weeks ($p < 0.01$) (Fig. 6D). The level was significantly reduced in the dbT1 and dbT2 groups in a dose-dependent manner ($p < 0.05$ db mice vs. dbT1 mice, $p < 0.01$ db mice vs. dbT2 mice), and the level in the dbF group was equivalent to that in the dbT1 group ($p < 0.05$ db mice vs. dbF mice).

3.10. XOR activity and concentrations of urate in the sciatic nerve, DRG and blood plasma (Fig. 7 and Suppl. Fig. 5)

XOR activity in the sciatic nerve and blood plasma was significantly increased compared with db/m mice at 4 weeks of treatment ($p < 0.05$ and $p < 0.01$, respectively) (Fig. 7A). Compared with db/m mice, a significant increase in XOR activity was observed in DRG tissues and blood plasma from db mice at 8 weeks ($p < 0.05$, respectively) (Fig. 7B). These elevated activities were significantly reduced in groups treated with XO inhibitors, as detected in the dbT1, dbT2 and dbF groups (Fig. 7A–B). Notably, the activity was partially dose-dependently suppressed in the dbT1 and dbT2 groups but only modestly suppressed in the dbF group. Consistent with the level of XOR activity, the UA contents in the DRG at 4 weeks and sciatic nerve at 8 weeks were comparable in db and db/m mice (Suppl. Fig. 5A–B). In contrast, UA contents in the plasma and sciatic nerve at 4 weeks, and plasma and DRG at 8 weeks were significantly increased in db mice compared to those in db/m mice ($p < 0.05$ for the sciatic nerve and $p < 0.01$ for DRG and plasma). Mice treated with topiroxostat showed a dose-dependent decrease in the UA content in the DRG at 8 weeks and the UA content was almost completely undetectable in the sciatic nerve in the dbT1 and dbF groups. The effects on plasma UA levels were modest in the dbF group. Immunostaining revealed XOR expression predominantly in endoneurial microvessels in the DRG, perineurium, and endoneurial and epineurial microvessels in the sciatic nerve (Fig. 7C–D). XOR expression in neuronal cells in the DRG was equivocal and much weaker than that in blood vessels.

4. Discussion

In this study, we systematically documented the beneficial effects of an XO inhibitor, topiroxostat, on the spontaneous development of neuropathy in db mice. First, we confirmed the effects of topiroxostat on suppressing macrophage activation and preventing the decrease in neurite outgrowth induced by XO exposure in vitro. Consistent with the effects of allopurinol on rats with experimental diabetes, topiroxostat protected against the progressive deterioration of both sensory and motor nerve conduction and elevated the pain sensation threshold in db mice, accompanied by the suppression of M1 macrophage infiltration and oxidative stress in the sciatic nerve in a dose-dependent manner (Inkster et al., 2007). In addition, we obtained structural evidence of its protective effect on neuropathy development in db mice treated with high-dose (2 mg/kg/day) topiroxostat based on the preservation of cutaneous small nerve fibers. The prevention of nerve fiber loss was not sufficient in the low-dose (1 mg/kg/day) topiroxostat or febuxostat group. The effects of XO inhibitors were independent of blood glucose control because hyperglycemia was sustained in the treated group. Based on the current results, we suggest several novel underlying mechanisms for the beneficial effects of topiroxostat on the development of diabetic neuropathy.

Conti et al. reported that macrophages transiently infiltrated the sciatic nerve in the early stages of a type 1 diabetic model, which may be involved in the regeneration of nerve tissue in response to nerve injury exerted by acute changes in glucose metabolism (Conti et al., 2002). In contrast, we first clarified that the transient migration of macrophages at the developing stage of T2D in db mice was mainly composed of M1

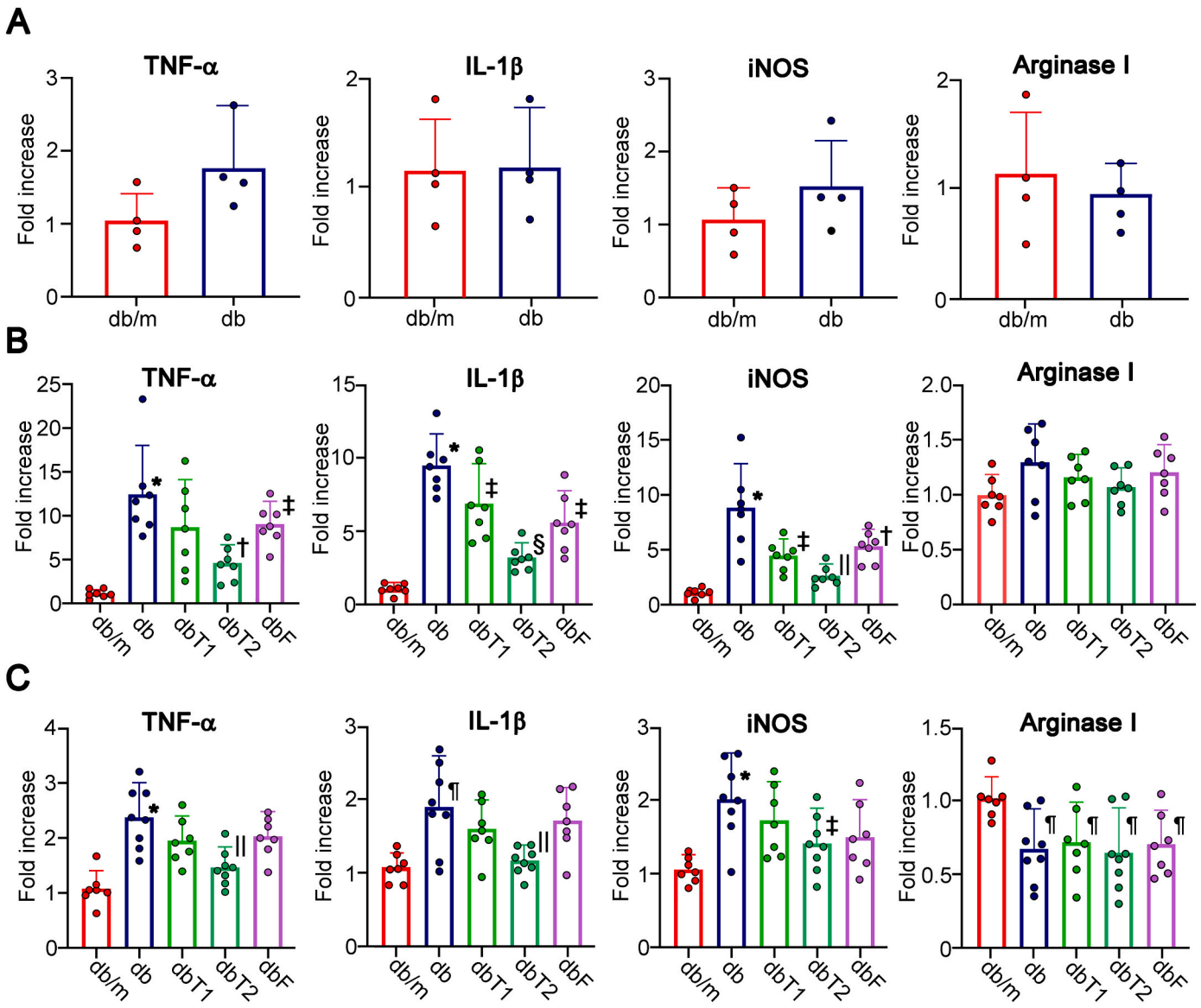

Fig. 4. mRNA expression of pro- and anti-inflammatory molecules in the sciatic nerve.
The mRNA expression levels of proinflammatory markers (TNF-α, IL-1β, and iNOS) and an anti-inflammatory marker (arginase I) in the sciatic nerve were comparable between db and db/m mice at baseline **(A)**. The expression of proinflammatory markers was 10 times greater in db mice than in db/m mice at 4 weeks ($p < 0.01$) (**B**). A dose-dependent decrease in the expression of proinflammatory markers was observed in the topiroxostat-treated groups. The febuxostat-treated group also showed reduced expression but to a lesser extent than the dbT2 group. Arginase I expression was similar among all the groups. The expression of proinflammatory molecules was much lower at 8 weeks but still higher in db mice than in db/m mice (**C**). The effects of treatment showed a similar trend to the changes observed at 4 weeks. Values are presented as means±SD. db/m, untreated db/m mice; db, db/db mice; dbT1, 1 mg/kg topiroxostat-treated db mice; dbT2, 2 mg/kg topiroxostat-treated db mice; dbF, febuxostat-treated db mice. $^{*}p < 0.01$ compared with db/m mice, $^{\dagger}p < 0.01$ compared with db mice, $^{\ddagger}p < 0.05$ compared with db mice, $^{\S}p < 0.01$ compared with db mice, $p < 0.05$ compared with the dbT1 and dbF groups, $^{||}p < 0.01$ compared with db mice, $p < 0.05$ compared with dbF mice, and $^{\P}p < 0.05$ compared with db/m mice.

macrophages that evoked neuronal dysfunction, such as delays in MNCV and SNCV and elevations in oxidative stress. Since XO activity is correlated with insulin resistance and factors associated with metabolic syndrome (Sunagawa et al., 2019), increased XO activity in plasma likely elicits the dominant M1 polarization of migrated macrophages in the injured sciatic nerve of db mice, as shown in our in vitro results. Subsequently, migrated M1 macrophages increase XO activity in the sciatic nerves of db mice at 4 weeks because XO is rapidly activated and accompanied by macrophage activation (Ives et al., 2015). Since XO inhibitors selectively suppress M1 macrophage infiltration and polarization but not M2 macrophage infiltration, XO inhibitors not only suppress neuronal damage but also promote neuronal regeneration in early DN lesions.

Intriguingly, M2 macrophage infiltration was gradually reduced in the sciatic nerve of db mice compared to db/m mice during disease development. Conversely, the M1/M2 ratio in db mice was markedly increased at 8 weeks compared with that at 4 weeks, despite a reduction in the absolute number of migrating M1 macrophages. Thus, acute inflammation may shift to chronic inflammation, which is commonly observed in diabetes and DN models (Fan et al., 2020; Khanna et al., 2010; Mizukami et al., 2011; Yamagishi et al., 2008). Although the levels of oxidative stress and inflammatory cytokines at 8 weeks of treatment were mild compared to those at 4 weeks, nerve tissues are chronically damaged with less regenerative ability, resulting in a reduction in IENFD.

In this study, the macrophage phenotype was classified as M1 or M2.

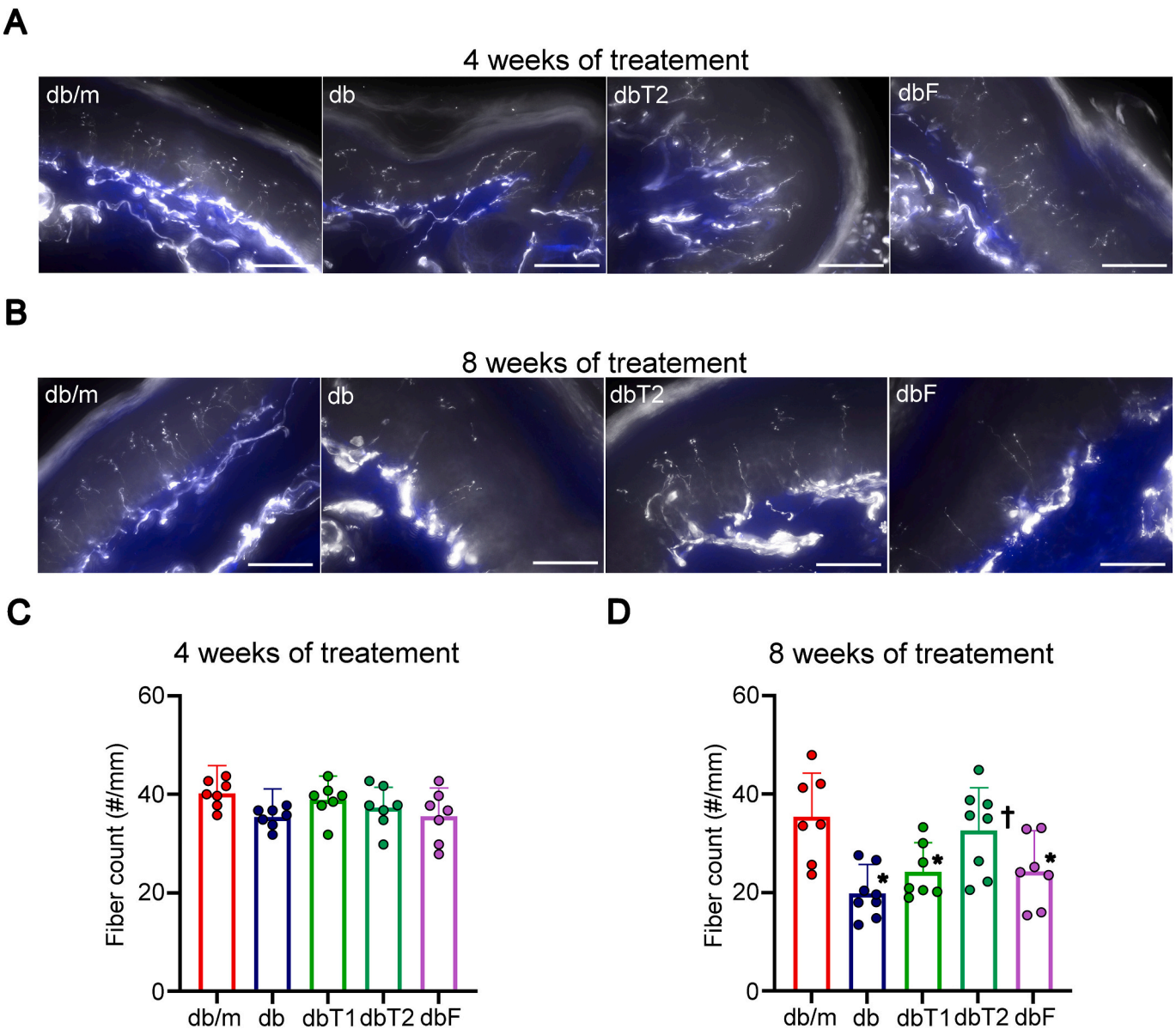

Fig. 5. Alterations in the intraepidermal nerve fiber density (IENFD).
Dermal and intraepidermal nerve fibers were visualized using double immunofluorescence staining for protein gene product 9.5 (PGP9.5) and cytokeratin 5/6 (CK5/6) to label nerve fibers (white) and the dermis (blue), respectively (**A–B**). The IENFD was comparable among all the mouse groups at 4 weeks (**A and D**). The IENFD of db mice was significantly reduced compared with that of db/m mice at 8 weeks ($p < 0.01$ compared with db/m mice) (**B and D**). Among the groups treated with XO inhibitors, the IENFD of the dbT2 group was significantly improved compared with that of db mice ($p < 0.05$ compared with db mice). Values are presented as means±SD. db/m, untreated db/m mice; db, db/db mice; dbT1, 1 mg/kg topiroxostat-treated db mice; dbT2, 2 mg/kg topiroxostat-treated db mice; dbF, febuxostat-treated db mice. *$p < 0.01$ compared with db/m mice, $^{\dagger}p < 0.01$ compared with db mice, and $p < 0.05$ compared with the dbT1 and dbF groups. The scale bar represents 50 μm. (For interpretation of the references to colour in this figure legend, the reader is referred to the web version of this article.)

Our results showed that the number of infiltrated M1 macrophages was significantly increased in the sciatic nerve during the early stage of DN and that the balance of M1/M2 macrophages was disturbed in the subsequent chronic stage of DN. Likewise, several reports have shown that the pathophysiology depends on this classification in various peripheral nerve diseases, including DN, while this classification is possibly too simplified. Xue et al. extended the current M1 versus M2 polarization model to a "spectrum model" with at least nine distinct macrophage activation programs (Xue et al., 2014). If this model is applied in the future, the pathophysiology of DN would be more completely elucidated in association with its stage and severity than that obtained based on the results from the present study.

Cheng et al. showed that db/db mice develop mechanical hyperalgesia during the early stage of diabetes (6–12 weeks of age) (Cheng et al., 2009). The mechanism was mediated by the upregulation of NGF signaling in the DRG along with increased levels of TNF-α and iNOS and interactions with neurons in the spinal cord (Cheng et al., 2012; Dauch et al., 2012). Intriguingly, the duration of mechanical hyperalgesia was consistent with the transient migration of M1 macrophages and increased production of proinflammatory cytokines in the sciatic nerve of db mice. Kiguchi et al. reported that M1 macrophage infiltration in the sciatic nerve evoked tactile allodynia, which was ameliorated by M2 polarization (Kiguchi et al., 2015). As shown in our study, XO activation is involved in M1 polarization in the sciatic nerve of db mice, suggesting that XO inhibitors would be a new therapeutic option for mechanical hyperalgesia in the early stage of DN.

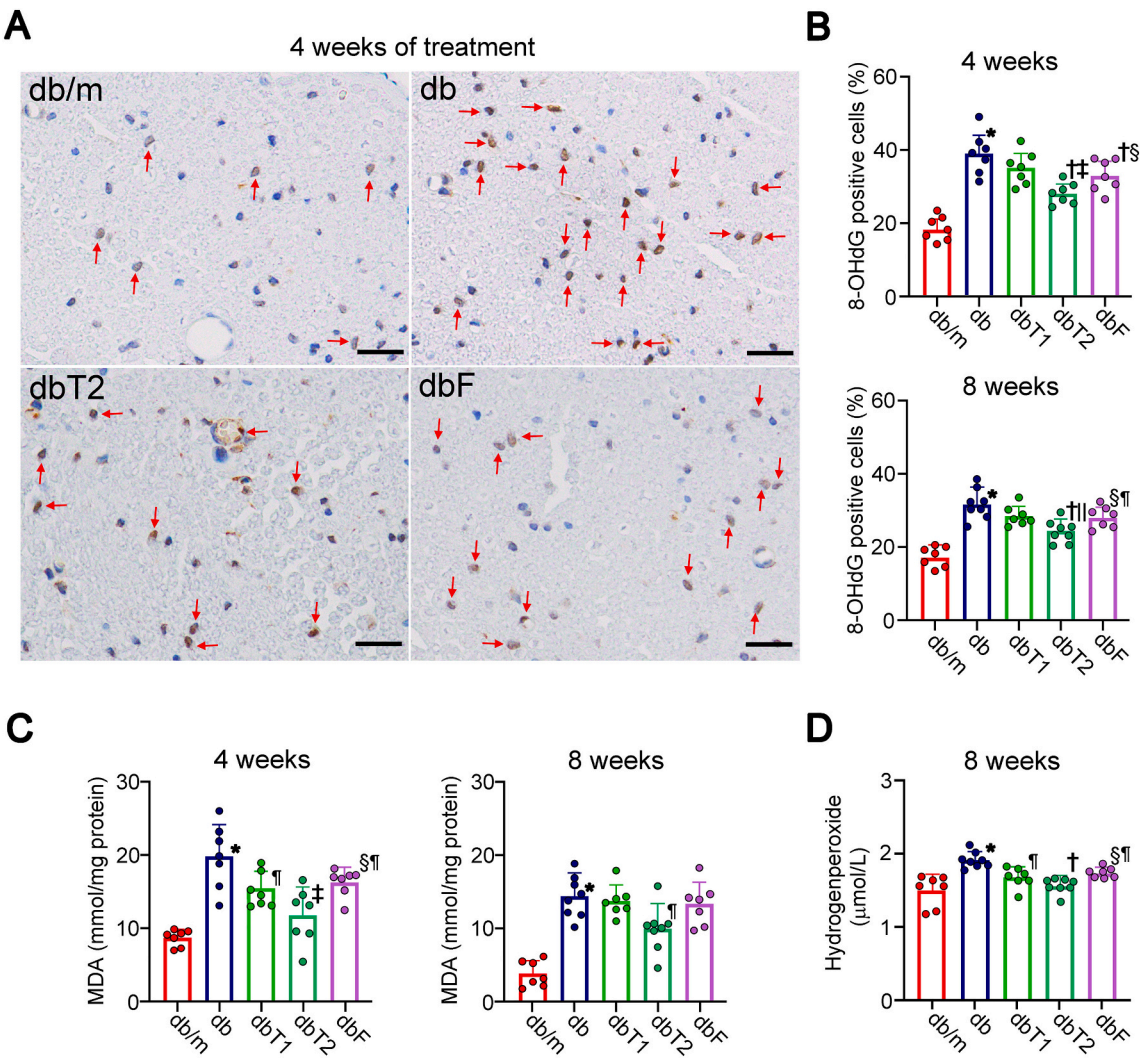

Fig. 6. Oxidative stress in the sciatic nerve.
Schwann cells with nuclei positive for 8-hydroxy-2′-deoxyguanosine (8-OHdG) were distributed diffusely in the sciatic nerve of db mice, whereas they were less frequently observed in db/m mice at 4 weeks of treatment **(A)**. Positive reactions were also observed in endothelial cells and macrophages. The frequency of positive cells was significantly increased in db mice at 4 weeks compared to db/m mice (**A–B**). The frequency of positive cells was decreased with treatment of torpiroxostat in a dose-dependent manner. Febuxostat treatment suppressed the frequency to a comparative level of that of the dbT1 group. Similar results were observed at 8 weeks, but the effect on the dbF group was weaker than on the dbT2 group (**B**). A dose-dependent decrease in malondialdehyde (MDA) levels was observed in the dbT1 and dbT2 groups at 4 and 8 weeks (**C**). The effect of febuxostat was comparable to that of dbT1. Plasma hydrogen peroxide levels in db mice were significantly higher than those in db/m mice at 8 weeks ($p < 0.01$) (**D**). The increase in plasma hydrogen peroxide levels was dose-dependently inhibited in the dbT1 and dbT2 groups and modestly inhibited in the dbF group ($p < 0.05$ db vs. db T1, $p < 0.01$ db vs. dbT2, and $p < 0.05$ db vs. dbF). db/m, untreated db/m mice; db, db/db mice; dbT1, 1 mg/kg topiroxostat-treated db mice; dbT2, 2 mg/kg topiroxostat-treated db mice; dbF, febuxostat-treated db mice. Values are presented as means±SD. *$p < 0.01$ compared with the db/m mice, $^{\dagger}p < 0.01$ compared with db mice, $^{\ddagger}p < 0.01$ compared with the dbT1 group, $^{\S}p < 0.05$ compared with the dbT2 group, $^{||}p < 0.05$ compared with the dbT1 group, $^{\P}p < 0.05$ compared with db mice. The scale bar represents 20 μm.

As repeatedly emphasized, excess ROS production is a cardinal cause of vascular and neurological complications of diabetes. In this study, we observed an increased population of 8-OHdG-positive cells in the sciatic nerve of db mice and a dose-dependent inhibition of their emergence by topiroxostat treatment. Activation of XO in the blood and nerve tissues results in excessive oxygen radical production, such as hydrogen peroxide and MDA, possibly leading to vascular and nerve tissue damage. Therefore, topiroxostat likely efficiently suppressed XO activity to prevent ROS production, resulting in sound nerve tissues. In fact, our study identified XO localization in endoneurial vessel walls and less clearly in Schwann cells or DRG neurons. XO activity was indeed elevated in blood plasma, sciatic nerve and DRG, and topiroxostat dose-dependently suppressed the activity of this enzyme, rescuing ROS-induced cell damage. Differences in the suppressive effects of topiroxostat and febuxostat on XO activity may indeed explain the potent protective effect of topiroxostat but not febuxostat on neuropathic changes.

Intriguingly, XO activity was not always observed at high levels in diabetic tissues, similar to the tissue concentration of urate. Although XO activities in the sciatic nerve were greater in db mice than in db/m mice at 4 weeks of treatment, activities in the DRG were similar. On the other hand, XO activities in the DRG were greater in db mice than in db/m mice at 8 weeks of treatment. The tissue urate concentration supported these changes in nerve tissues. The reason for this discrepancy among the tissues is not known. However, in the case of the sciatic nerve, transient macrophage infiltration may be ascribed to the increase in XO activities, because XO activities are abundantly detected in activated macrophages (Ives et al., 2015). Regarding the DRG, we speculate that the topographical localization of XO predominantly in the vascular wall indicates that tissue blood flow may be critical for urate

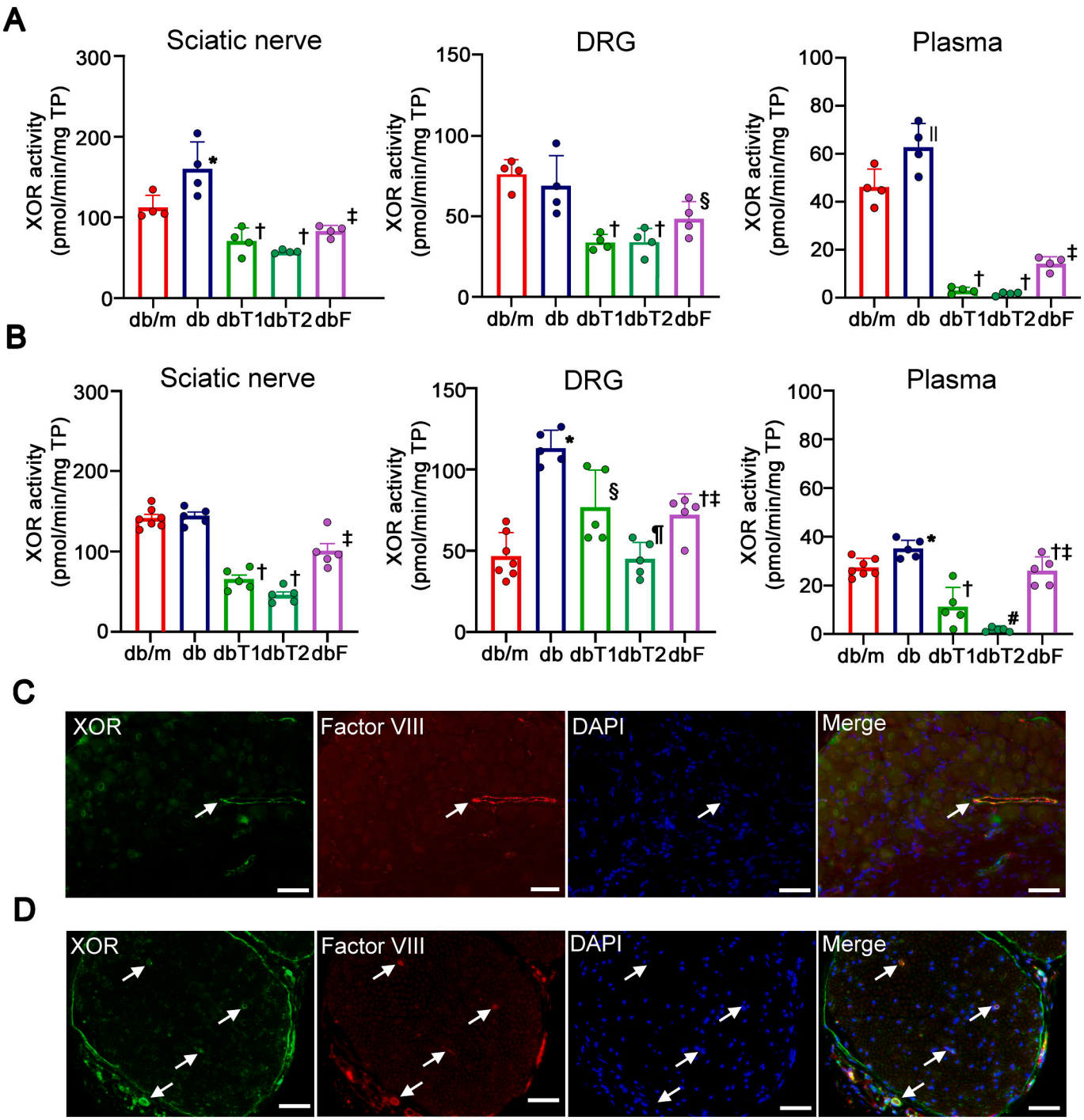

Fig. 7. Tissue XOR activity and localization of XOR.
XOR activity was elevated in the sciatic nerve and plasma of db mice, but was comparable in the DRG between db/m and db mice at 4 weeks. (**A**). XOR activity was elevated in the DRG and plasma of db mice, but comparable in the sciatic nerve between db/m and db mice at 8 weeks (**B**). XO inhibitors significantly suppressed the activation of XOR in the sciatic nerve, DRG and plasma of db mice at 4 and 8 weeks of treatment. Notably, topiroxostat suppressed XOR activity in plasma to a greater extent than febuxostat ($p < 0.01$ dbF vs. dbT2). XOR was expressed predominantly in factor VIII-positive-blood vessels in the sciatic nerve and DRG (white arrows) (**C–D**). Perineurial and epineurial microvessels were also positive in the DRG, but the reaction was equivocal in neuronal cells. Values are presented as means±SD. XOR, xanthine oxidoreductase; TP, total protein; db/m, untreated db/m mice; db, db/db mice; dbT1, 1 mg/kg topiroxostat-treated db mice; dbT2, 2 mg/kg topiroxostat-treated db mice; dbF, febuxostat-treated db mice. *$p < 0.05$ compared with db/m mice, †$p < 0.01$ compared with db mice, ‡$p < 0.01$ compared with dbT2 mice, §$p < 0.05$ compared with db mice, ||$p < 0.01$ compared with db/m mice, ¶$p < 0.01$ compared with dbT1 mice, and #$p < 0.05$ compared with dbT1 mice. The scale bar represents 100 μm.

accumulation. The DRG is rich in blood flow compared with the sciatic nerve, which is poorly vascularized (Zochodne and Ho, 1991). Considering the results of nerve conduction velocities and tail flick test, mice are in the developmental stage at 4 weeks of treatment (9 weeks of age). Therefore, microvessel expansion in the DRG might be immature. After the achievement of sufficient microvessel expansion at 8 weeks of treatment, a plausible hypothesis is that elevated blood XO activity promotes the production of oxidized products in the DRG, leading to

distal nerve fiber loss even without excess urate accumulation. We also showed that macrophages or DRG neurons are affected when exposed to environmental XO in vitro. Thus, rather than urate concentrations, environmental XO mostly originating from the blood appeared to be crucial for the genesis of complications in a mouse diabetes model.

In this study, we observed an increase in fasting blood glucose levels in mice treated with XO inhibitors compared to the untreated group. The reason for this phenomenon is not known, and we wonder whether high-dose topiroxostat potentially exerts adverse effects. However, the HbA1c, fasting insulin and fed blood glucose levels were all comparable among the untreated and treated db groups. The OGTT and ITT did not reveal any significant effects of the topiroxostat treatment on post-challenge glucose intolerance or insulin sensitivity, respectively. Based on these results, a serious worsening of glucose intolerance is not expected in subjects with diabetes treated with an XO inhibitor. A slight but significant reduction in body weight in db mice treated with high-dose topiroxostat may also be relevant to an improvement in morbidity. In fact, continuous lifestyle interventions for a year successfully inhibited the reduction of IENFD together with body weight reduction in subjects with impaired glucose tolerance (Smith et al., 2006).

Our study has some limitations. First, we assessed only the protective effects of XO inhibitors rather than the therapeutic effects. Neuropathy in individuals with T2D naturally develops from the prediabetic stage, but the clinical application of drug therapy, except for lifestyle interventions, is usually impractical. Hence, intervention studies must be conducted on models with established neuropathy. Second, we did not explore the specific molecular mechanisms occurring in the inhibition of neuropathy by an XO inhibitor. Unfortunately, we were not able to access the gene targeting model of XO or amplified XO expression. Future studies examining the pathway from purine to urate and its relation to peripheral nerves are warranted. Finally, the implication of leptin signaling in macrophage infiltration in the DN model was not explored in this study. An evaluation of DN in mice with diet-induced obesity treated with an XO inhibitor may provide useful information to answer this question.

5. Conclusions

XO inhibitors, particularly high doses of topiroxostat, exert protective effects on neuropathy development in db mice. Plasma XO activation promoted ROS generation, resulting in both direct and indirect peripheral nerve tissue injuries. We consider that plasma XO may be a novel target for the prevention of neuropathy development in patients with diabetes.

Ethical approval and consent to participate

The Committee on Animal Care of Hirosaki University approved all the experiments conducted in this study (#M14006). The procedures followed the Principles of Laboratory Animal Care (National Institutes of Health publication no. 85–23, revised 1985) and the institutional guidelines of Hirosaki University Animal Experimentation for the care and use of laboratory animals.

Consent for publication

Not applicable.

Availability of data and materials

The datasets used and/or analyzed during the current study are available from the corresponding author upon reasonable request.

Funding

This work was supported by Sanwa Kagaku Pharmacological Inc. Topiroxostat and febuxostat were kind gifts from Sanwa Kagaku Pharmacological Inc.

Declaration of Competing Interest

The authors have no competing interests to declare.

Acknowledgments

Technical assistance provided by Ms. Saeko Osanai, Misato Sakamoto, and Hiroko Mori of the Department Pathology and Molecular Medicine of Hirosaki University Graduate of Medicine is highly appreciated.

Appendix A. Supplementary data (Table 1 and Figure 1-5)

Supplementary data to this article can be found online at https://doi.org/10.1016/j.nbd.2021.105392.

References

Amaya, Y., et al., 1990. Proteolytic conversion of xanthine dehydrogenase from the NAD-dependent type to the O_2-dependent type; amino acid sequence of rat liver xanthine dehydrogenase and identification of the cleavage sites of the enzyme protein during irreversible conversion by trypsin. J. Biol. Chem. 265, 14170–14175.

Azmi, S., et al., 2015. Corneal confocal microscopy identifies small-Fiber neuropathy in subjects with impaired glucose tolerance who develop type 2 diabetes. Diabetes Care 38, 1502–1508. https://doi.org/10.2337/dc14-2733.

Cheng, H.T., et al., 2009. Nerve growth factor mediates mechanical allodynia in a mouse model of type 2 diabetes. J. Neuropathol. Exp. Neurol. 68, 1229–1243. https://doi.org/10.1097/NEN.0b013e3181bef710.

Cheng, H.T., et al., 2012. Nerve growth factor/p38 signaling increases intraepidermal nerve fiber densities in painful neuropathy of type 2 diabetes. Neurobiol. Dis. 45, 280–287. https://doi.org/10.1016/j.nbd.2011.08.011.

Conti, G., et al., 2002. Macrophage infiltration and death in the nerve during the early phases of experimental diabetic neuropathy: a process concomitant with endoneurial induction of IL-1beta and p75NTR. J. Neurol. Sci. 195, 35–40. https://doi.org/10.1016/s0022-510x(01)00684-0.

Dauch, J.R., et al., 2012. Neuron-astrocyte signaling network in spinal cord dorsal horn mediates painful neuropathy of type 2 diabetes. Glia. 60, 1301–1315. https://doi.org/10.1002/glia.22349.

Fan, B., et al., 2020. Mesenchymal stromal cell-derived exosomes ameliorate peripheral neuropathy in a mouse model of diabetes. Diabetologia. 63, 431–443. https://doi.org/10.1007/s00125-019-05043-0.

Feldman, E.L., et al., 2017. New horizons in diabetic neuropathy: mechanisms, bioenergetics, and pain. Neuron. 93, 1296–1313. https://doi.org/10.1016/j.neuron.2017.02.005.

Furuhashi, M., et al., 2018. Plasma xanthine oxidoreductase activity as a novel biomarker of metabolic disorders in a general population. Circ. J. 82, 1892–1899. https://doi.org/10.1253/circj.CJ-18-0082.

Guo, D., et al., 2020. Beneficial effects of combination therapy of canagliflozin and teneligliptin on diabetic polyneuropathy and β-cell volume density in spontaneously type 2 diabetic Goto-Kakizaki rats. Metabolism. 107, 154232. https://doi.org/10.1016/j.metabol.2020.154232.

Honorat, J.A., et al., 2013. Xanthine oxidase mediates axonal and myelin loss in a murine model of multiple sclerosis. PLoS One 8, e71329. https://doi.org/10.1371/journal.pone.00713.

Inkster, M.E., et al., 2007. Treatment with the xanthine oxidase inhibitor, allopurinol, improves nerve and vascular function in diabetic rats. Eur. J. Pharmacol. 561, 63–71. https://doi.org/10.1016/j.ejphar.2006.12.029.

Ives, A., et al., 2015. Xanthine oxidoreductase regulates macrophage IL1β secretion upon NLRP3 inflammasome activation. Nat. Commun. 6, 6555. https://doi.org/10.1038/ncomms7555.

Juranek, J.K., et al., 2013. RAGE deficiency improves postinjury sciatic nerve regeneration in type 1 diabetic mice. Diabetes. 62, 931–943. https://doi.org/10.2337/db12-0632.

Khanna, S., et al., 2010. Macrophage dysfunction impairs resolution of inflammation in the wounds of diabetic mice. PLoS One 5, e9539. https://doi.org/10.1371/journal.pone.0009539.

Kiguchi, N., et al., 2015. Peripheral interleukin-4 ameliorates inflammatory macrophage-dependent neuropathic pain. Pain. 156, 684–693. https://doi.org/10.1097/j.pain.0000000000000097.

Kudoh, K., et al., 2020. Lipopolysaccharide-binding protein is a distinctive biomarker of abnormal pain threshold in the general Japanese population. BMJ Open Diabetes Res. Care 8, e001739. https://doi.org/10.1136/bmjdrc-2020-001739.

Mehra, S., et al., 2007. Corneal confocal microscopy detects early nerve regeneration after pancreas transplantation in patients with type 1 diabetes. Diabetes Care 30, 2608–2612. https://doi.org/10.2337/dc07-0870.

Miric, D.J., et al., 2016. Xanthine oxidase activity in type 2 diabetes mellitus patients with and without diabetic peripheral neuropathy. J. Diabetes Res. 2016, 4370490. https://doi.org/10.1155/2016/4370490.

Mizukami, H., et al., 2011. Methylcobalamin effects on diabetic neuropathy and nerve protein kinase C in rats. Eur. J. Clin. Investig. 41, 442–450. https://doi.org/10.1111/j.1365-2362.2010.02430.x.

Mizukami, H., et al., 2020. Role of glucosamine in development of diabetic neuropathy independent of the aldose reductase pathway. Brain Commun. 2, fcaa168 https://doi.org/10.1093/braincomms/fcaa168.

Murase, T., et al., 2016. A highly sensitive assay of human plasma xanthine oxidoreductase activity using stable isotope-labeled xanthine and LC/TQMS. J. Chromatogr. B Analyt. Technol. Bomed. Life Sci. 1039, 51–58. https://doi.org/10.1016/j.jchromb.2016.10.033.

Nakamura, T., et al., 2016. Effects of topiroxostat and febuxostat on urinary albumin excretion and plasma xanthine oxidoreductase activity in db/db mice. Eur. J. Pharmacol. 780, 224–231. https://doi.org/10.1016/j.ejphar.2016.03.055.

Nakamura, T., et al., 2019. The influence of albumin on the plasma xanthine oxidoreductase inhibitory activity of allopurinol, febuxostat and topiroxostat: insight into extra-urate lowering effect. Integr Mol Med 6, 1–7. https://doi.org/10.15761/IMM.1000368.

Nishikawa, T., et al., 2020. Xanthine oxidase inhibition attenuates insulin resistance and diet-induced steatohepatitis in mice. Sci. Rep. 10, 815. https://doi.org/10.1038/s41598-020-57784-3.

Norido, F., et al., 1984. Development of diabetic neuropathy in the C57BL/Ks (db/db) mouse and its treatment with gangliosides. Exp. Neurol. 83, 221–232. https://doi.org/10.1016/S0014-4886(84)90094-3.

O'Brien, P.D., et al., 2015. BTBR ob/ob mice as a novel diabetic neuropathy model: neurological characterization and gene expression analyses. Neurobiol. Dis. 73, 348–355. https://doi.org/10.1016/j.nbd.2014.10.015.

Okuda, S., et al., 1996. Hydrogen peroxide-mediated neuronal cell death induced by an endogenous neurotoxin, 3-Hydroxykynurenine proc. Natl. Acad. Sci. U. S. A. 93, 12553–12558. https://doi.org/10.1073/pnas.93.22.12553.

Sango, K., et al., 2008. Neuroprotective properties of ciliary neurotrophic factor for cultured adult rat dorsal root ganglion neurons. Histochem. Cell Biol. 130, 669–679. https://doi.org/10.1007/s00418-008-0484-x.

Sango, K., et al., 2011. Spontaneously immortalized Schwann cells from adult Fischer rat as a valuable tool for exploring neuron-Schwann cell interactions. J. Neurosci. Res. 89, 898–908. https://doi.org/10.1002/jnr.22605.

Smith, A.G., et al., 2006. Lifestyle intervention for pre-diabetic neuropathy. Diabetes Care 29, 1294–1299. https://doi.org/10.2337/dc06-0224.

Sunagawa, S., et al., 2019. Activity of xanthine oxidase in plasma correlates with indices of insulin resistance and liver dysfunction in patients with type 2 diabetes mellitus and metabolic syndrome: a pilot exploratory study. J Diab. Invest. 10, 94–103. https://doi.org/10.1111/jdi.12870.

Takahashi, K., et al., 2012. A melioration of acute kidney injury in lipopolysaccharide-induced systemic inflammatory response syndrome by an aldose reductase inhibitor, fidarestat. PLoS One 7, e30134. https://doi.org/10.1371/journal.pone.0030134.

Tsuboi, K., et al., 2016. The dipeptidyl peptidase IV inhibitor vildagliptin suppresses development of neuropathy in diabetic rodents: effects on peripheral sensory nerve function, structure and molecular changes. J. Neurochem. 136, 859–870. https://doi.org/10.1111/jnc.13439.

Vinik, A.I., et al., 2013. Diabetic neuropathy. Endocrinol. Metab. Clin. N. Am. 42, 747–787. https://doi.org/10.1016/j.ecl.2013.06.001.

Xue, J., et al., 2014. Transcriptome-based network analysis reveals a spectrum model of human macrophage activation. Immunity. 40, 274–288. https://doi.org/10.1016/j.immuni.2014.01.006.

Yagihashi, S., et al., 2011. Mechanism of diabetic neuropathy: where are we now and where to go? J Diab. Invest. 2, 18–32. https://doi.org/10.1111/j.2040-1124.2010.00070.x.

Yamagishi, S., et al., 2008. Correction of protein kinase C activity and macrophage migration in peripheral nerve by pioglitazone, peroxisome proliferator activated-gamma-ligand, in insulin-deficient diabetic rats. J. Neurochem. 104, 491–499. https://doi.org/10.1111/j.1471-4159.2007.05050.x.

Ziegler, D., et al., 2014. Epidemiology of polyneuropathy in diabetes and prediabetes. Handb. Clin. Neurol. 126, 3–22. https://doi.org/10.1016/B978-0-444-53480-4.00001-1.

Zochodne, D.W., Ho, L.T., 1991. Unique microvascular characteristics of the dorsal root ganglion in the rat. Brain Res. 559, 89–93. https://doi.org/10.1016/0006-8993(91)90290-c.